

Principle of subtraction ghost imaging in scattering medium

Qin Fu(付芹), Yanfeng Bai(白艳锋), Wei Tan(谭威), Xianwei Huang(黄贤伟), Suqin Nan(南苏琴), and Xiquan Fu(傅喜泉)

Citation: Chin. Phys. B, 2023, 32 (**6**): 064203. DOI: 10.1088/1674-1056/acb202
Journal homepage: http://cpb.iphy.ac.cn; http://iopscience.iop.org/cpb

What follows is a list of articles you may be interested in

A probability theory for filtered ghost imaging

Zhong-Yuan Liu(刘忠源), Shao-Ying Meng(孟少英), and Xi-Hao Chen(陈希浩)
Chin. Phys. B, 2023, 32 (**4**): 044204. DOI: 10.1088/1674-1056/ac981e

Ghost imaging based on the control of light source bandwidth

Zhao-Qi Liu(刘兆骐), Yan-Feng Bai(白艳锋), Xuan-Peng-Fan Zou(邹璇彭凡), Li-Yu Zhou(周立宇), Qin Fu(付芹), and Xi-Quan Fu(傅喜泉)
Chin. Phys. B, 2023, 32 (**3**): 034210. DOI: 10.1088/1674-1056/ac6edd

Orthogonal-triangular decomposition ghost imaging

Jin-Fen Liu(刘进芬), Le Wang(王乐), and Sheng-Mei Zhao(赵生妹)
Chin. Phys. B, 2022, 31 (**8**): 084202. DOI: 10.1088/1674-1056/ac5e99

Imaging a periodic moving/state-changed object with Hadamard-based computational ghost imaging

Hui Guo(郭辉), Le Wang(王乐), and Sheng-Mei Zhao(赵生妹)
Chin. Phys. B, 2022, 31 (**8**): 084201. DOI: 10.1088/1674-1056/ac6498

Efficient implementation of x-ray ghost imaging based on a modified compressive sensing algorithm

Haipeng Zhang(张海鹏), Ke Li(李可), Changzhe Zhao(赵昌哲), Jie Tang(汤杰), and Tiqiao Xiao(肖体乔)
Chin. Phys. B, 2022, 31 (**6**): 064202. DOI: 10.1088/1674-1056/ac48f7

Principle of subtraction ghost imaging in scattering medium

Qin Fu(付芹)[1], Yanfeng Bai(白艳锋)[1,†], Wei Tan(谭威)[1],
Xianwei Huang(黄贤伟)[1], Suqin Nan(南苏琴)[2], and Xiquan Fu(傅喜泉)[1,‡]

[1] *College of Computer Science and Electronic Engineering, Hunan University, Changsha* 410082, *China*
[2] *School of Computer and Information Engineering, Hunan University of Technology and Business, Changsha* 410205, *China*

(Received 8 September 2022; revised manuscript received 8 January 2023; accepted manuscript online 11 January 2023)

Scattering medium in light path will cause distortion of the light field, resulting in poor signal-to-noise ratio (SNR) of ghost imaging. The disturbance is usually eliminated by the method of pre-compensation. We deduce the intensity fluctuation correlation function of the ghost imaging with the disturbance of the scattering medium, which proves that the ghost image consists of two correlated results: the image of scattering medium and the target object. The effect of the scattering medium can be eliminated by subtracting the correlated result between the light field after the scattering medium and the reference light from ghost image, which verifies the theoretical results. Our research may provide a new idea of ghost imaging in harsh environment.

Keywords: ghost imaging, image reconstruction techniques, scattering medium

PACS: 42.50.–p, 42.30.–d, 42.25.Dd, 42.25.Fx **DOI:** 10.1088/1674-1056/acb202

1. Introduction

Ghost imaging (GI) is an optical technique which retrieves an unknown object via intensity correlation of two correlated light beams. The first GI experiment was performed by using entangled photon pairs produced by spontaneous parametric down conversion.[1] Later, it was shown that GI could also be realized with a classical thermal light source.[2] Subsequently, GI has been widely investigated and some new methods have been introduced to improve imaging quality, such as high-order GI,[3] pseudo-inverse GI,[4] differential ghost imaging (DGI)[5] and compressive ghost imaging (CSGI).[6] In addition, machine learning[7–10] has attracted much attention in GI since ghost image under a low sampling condition can be quickly and accurately acquired.[11]

For a realistic imaging system, the light beam can be influenced by various harsh environment disturbances, such as atmospheric turbulence,[12] scattering medium,[13–15] the bending in fibers,[16,17] which cause degradation of imaging quality. To eliminate the effect of the negative factors on the light beam, a great number of pre-compensation techniques have been developed, such as adaptive optics[18] and feedback wavefront shaping.[19,20] However, several problems limit high-speed and robust applications of these techniques. On the one hand, these techniques require sophisticated hardware support, such as ultra-fast processor, low-noise sensor, and expensive SLM. On the other hand, the imaging process suffers from fussy calibration and time-consuming scanning over the whole field of view. In this paper, we theoretically verify that the imaging result under the disturbance of the scattering medium can be regarded as the superposition of two correlated results of scattering medium image and target image. To prove the conclusion, the effect of the medium can be eliminated experimentally and numerically by subtracting the correlation result between the reference light field and the field disturbed by the scattering medium from ghost image. Additionally, GI with the scattering medium at the different positions is implemented theoretically and experimentally to verify the effectiveness of the scheme. The scheme avoids the complicated pre-compensation process and may be applied not only to environment with scattering but also to other disturbance channels.

2. Theoretical analysis

We firstly verify the correctness of the scheme in principle. Figure 1 shows the setup of reflective GI with the scattering medium. The light beam impinges on a slowly rotating ground glass to generate the pseudo-thermal light source,[21,22] and then a beam splitter (BS_1) divides the spatially incoherent light beam into two parts (the test beam and the reference beam). In the reference arm, the light freely propagates z_0 to a charge-coupled device (CCD) camera D_r. In the test arm, the light transmits through the scattering medium which is located at z_3 and propagates z_4 to the target object. Then, all reflected photons from the object are collected by a bucket detector D_{t2}. According to the optical coherence, the information of the object in GI is completely included in the intensity fluctuation correlation function[2]

$$G(x_r,x_t) \propto \left| \int \langle E^*(u_1)E(u_2)\rangle h_r(u_1,x_r)h_t^*(u_2,x_t)\,\mathrm{d}u_1\,\mathrm{d}u_2 \right|^2, \quad (1)$$

†Corresponding author. E-mail: yfbai@hnu.edu.cn
‡Corresponding author. E-mail: fuxq@hnu.edu.cn

© 2023 Chinese Physical Society and IOP Publishing Ltd

where u_1 and u_2 represent the transverse coordinates of the source plane, $h_{\rm r}(u_1,x_{\rm r}) \propto \exp\left[-\frac{{\rm j}\pi}{\lambda z_0}(x_{\rm r}-u_1)^2\right]$ is the impulse response function of the reference path, and $h_{\rm t}^*(u_2,x_{\rm t})$ denotes the phase conjugate of the impulse response function in the test path. Suppose that the source is spatially incoherent and satisfies $\langle E^*(u_1)E(u_2)\rangle = I_0\delta(u_1-u_2)$, where $\delta(\cdot)$ is the delta function. In the test arm, the scattering medium divides the distance between the source and the object into z_3 and z_4. Then, the impulse response function with the disturbance of the scattering medium in the test path[13] can be expressed as

$$\begin{aligned}
&h_{\rm t}(u_2,x_{\rm t})\\
\propto\ &\alpha h_{\rm i}(u_2,x_{\rm t})+\beta h_{\rm s}(u_2,x_{\rm t})\\
=\ &\int {\rm d}\xi\left\{\alpha\exp\left[-\frac{{\rm j}\pi}{\lambda(z_3+z_4)}(\xi\cos\theta_{\rm i}-u_2)^2\right]\right.\\
&+\beta\int {\rm d}x_1\,{\rm d}x_2\exp\left[-\frac{{\rm j}\pi}{\lambda z_3}(x_1-u_2)^2\right]\\
&\times\exp({\rm j}\phi(x_1))\exp\left[-\frac{{\rm j}\pi}{\lambda\Delta z}(x_1-x_2)^2\right]\exp({\rm j}\phi(x_2))\\
&\left.\times\exp\left[-\frac{{\rm j}\pi}{\lambda(z_4-\Delta z)}(\xi\cos\theta_{\rm i}-x_2)^2\right]\right\}t(\xi)\\
&\times\exp\left[-\frac{{\rm j}\pi}{\lambda z_2}(x_{\rm t}-\xi\cos\theta_{\rm o})^2\right]. \qquad (2)
\end{aligned}$$

The above formula denotes the sum of the impulse response function without the scattering $h_{\rm i}(u_2,x_{\rm t})$ and the multiple scattering $h_{\rm s}(u_2,x_{\rm t})$. In Eq. (2), $\theta_{\rm i}$ and $\theta_{\rm o}$ signify the incident angle and the reflective angle, respectively; α and β represent the probability amplitudes of the incident light and the scattering light, respectively, and satisfy the relation $\alpha+\beta=1$; $t(\xi)$ is the reflective function of target, ξ is the coordinate on the object plane; x_1 and x_2 represent the coordinates on the incident plane and the output plane of the scattering medium, respectively. The distance between those two planes is Δz; $\phi(x_1)$ and $\phi(x_2)$ denote the phase shifts of the random phase screen. Owing to the statistical property of the phase screen, the spatial auto-correlation function of each screen satisfies[23]

$$\begin{aligned}
\langle\exp\{{\rm j}\phi(x_1)-{\rm j}\phi(x_1')\}\rangle &= \exp\left\{-\sigma^2\left[1-{\rm e}^{-\frac{(x_1'-x_1)^2}{s^2}}\right]\right\}\\
&= \gamma(x_1,x_1'), \qquad (3)
\end{aligned}$$

where σ is the variance of the random phase screen and s denotes the correlation length of the phase screen. Since the length of the scattering medium is much shorter than that of the test arm, the length of the scattering medium can be ignored, i.e., $\Delta z = 0$. For the sake of simplifying the final equation, assume that the target object satisfies $\langle t(\xi)t^*(\xi')\rangle = T(\xi)\delta(\xi-\xi')$[24] and the scattering medium is close to the object. Substituting Eqs. (2) and (3) into Eq. (1) and using the related calculation methods in Ref. [25], the reconstructed result (ghost image of the target under the disturbance of the scattering medium) can be expressed as

$$\begin{aligned}
G(x_{\rm r}) \propto\ &\alpha\int {\rm d}\xi T(\xi){\rm sinc}^2\left[\frac{D(\xi\cos\theta_{\rm i}-x_{\rm r})}{\lambda z_0}\right]\\
&+\beta\int {\rm d}x_1\,{\rm d}x_1'\gamma(x_1,x_1')\\
&\times{\rm sinc}\left[\frac{D(x_1-x_{\rm r})}{\lambda z_3}\right]{\rm sinc}\left[\frac{D(x_{\rm r}-x_1')}{\lambda z_3}\right]\\
&\times{\rm sinc}\left[\frac{D(x_1-x_1')}{\lambda z_2}\right]\exp\left[-\frac{{\rm j}\pi(z_2+z_3)(x_1^2-x_1'^2)}{\lambda z_2 z_3}\right]\\
=\ &\alpha G'(x_{\rm r})+\beta G''(x_{\rm r}), \qquad (4)
\end{aligned}$$

where ${\rm sinc}(x)=\frac{\sin(\pi x)}{\pi x}$, and D is the effective transverse size of the detector. It is obvious that the reconstructed result includes two terms, $G'(x_{\rm r})$ and $G''(x_{\rm r})$, which represent GI of the target object without disturbance and the correlated result of the scattering medium, respectively. It is demonstrated that the scattering medium can be treated as a "new object", and the recovered image of the target object $G'(x_{\rm r})$ can be retrieved by subtracting correlated image of the scattering medium $G''(x_{\rm r})$ from ghost image $G(x_{\rm r})$, i.e.,

$$\alpha G'(x_{\rm r}) = G(x_{\rm r})-\beta G''(x_{\rm r}). \qquad (5)$$

3. Experiment and simulation verification

To prove Eq. (5), we design experiments in which we add another beam splitter (BS_2) behind the scattering medium. A bucket detector $D_{\rm t1}$ is used to record the light field after the scattering medium, which is shown in the dotted box of Fig. 1. In the experiment, the wavelength of the light beam $\lambda = 532$ nm. CCD camera $D_{\rm r}$ is Thorlabs: DCC3260C with 1216×1936 pixels, and bucket detectors $D_{\rm t1}$ and $D_{\rm t2}$ are Thorlabs PDA100A2 (detected area 75.4 mm^2, gain 70 dB). The positions of the bucket detectors are $z_1 = 40$ cm, and $z_2 = 50$ cm. A reflective double slit with smooth surface (slit width is 0.6 mm, a center-to-center separation is 0.8 mm, and the height is 0.9 mm) is used as target object. Here, a transparent cube glass with the side length $d = 40$ mm is full of the suspension liquid, the liquid is made up of the certain concentration of latex spherical calibration particles (GBW(E)12002a with the particle diameter 3.5 μm) and saturated NaCl solution (the density $\rho = 1.19$ g/cm^3), which is used to simulate the scattering medium. The position of the scattering medium in the test arm z_3 is normalized by its maximum values, i.e., $z_{\rm sa} = z_3/z_0$ (see Fig. 1). Here, $z_0 = z_3+z_4 = 100$ cm, $z_3 = 58$, 86, 95 cm, which correspond to $z_{\rm sa} = 0.58$, 0.86, 1, respectively. The lower the $z_{\rm sa}$ is, the closer the scattering medium is to the light source. The probability amplitudes of the scattering light $\beta = 0.5$, and the probability amplitudes of the incident light $\alpha = 0.5$. Here, β is calculated as the ratio of the sum of the scattered light to the sum of initial light. The more

the latex spherical calibration particles, the greater the β value. To quantitatively analyze the effectiveness of our scheme and to perform a more accurate comparison between the reconstructed image G and target object O, the correlation coefficient Corr is defined as[26]

$$\mathrm{Corr}(G,O)=\frac{\mathrm{Cov}(G,O)}{\sqrt{\mathrm{var}(G)\mathrm{var}(O)}}, \tag{6}$$

where $\mathrm{Cov}(G,O)$ means the covariance between the reconstructed image G and the object O, while $\mathrm{var}(G)$ and $\mathrm{var}(O)$ represent the corresponding variances, respectively. The higher the correlation coefficient is, the better the reconstruction image is. The Corr of every figure is marked at the bottom.

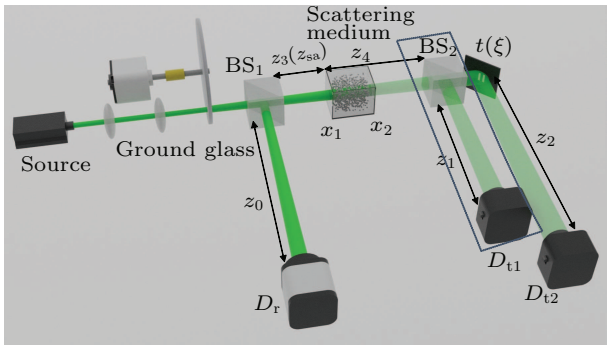


Fig. 1. Setup of reflective GI with the scattering medium in the test arm.

Figure 2(a1) shows the experimental result of ghost image when the scattering medium is close to the target object ($z_{\mathrm{sa}}\approx 1$), and GI without disturbance of the scattering medium is shown in Fig. 2(a3). It is obvious that the scattering medium deteriorates imaging quality greatly. The correlated result of the scattering medium can be obtained from the intensity correlation between the value of D_{t1} and CCD, as shown in Fig. 2(a2). For convenience of observation, part of noise is marked by black dotted box. It is obvious that the background noise of ghost image partly originates from the scattering medium by comparing the black dotted boxes in Figs. 2(a1) and 2(a2). After subtracting the correlated result of the scattering medium from ghost image directly, the recovered image is presented in Fig. 2(a4). One can see clearly that the corresponding noise can be eliminated, and the object information can be recovered greatly. Compared with Fig. 2(a3), the Corr of recovered image can reach 78%. To verify the effectiveness of the subtraction operation, considering two other cases in which the scattering medium is located at $z_{\mathrm{sa}}=0.86$ and 0.58. The Corr versus position z_{sa} is shown in Fig. 2(b). Compared with the two lines in Fig. 2(b), it is interesting to find that the subtraction operation is still effective and the Corr increases much after the subtraction operation. Here, Corr of the recovered image decreases with the decrease of z_{sa}, and the phenomenon can be explained according to defocusing theory.[27] As mentioned above, the scattering medium can be treated as an object. When the "new object" moves away from the target object, the condition of lensless GI, i.e., $z_0=z_3$ is not satisfied, and the defocusing length increases gradually, which deteriorates imaging quality of the "new object". Thus, the correlated result which is subtracted is not a perfect image of the scattering medium, thus the Corr of the subtraction scheme is finite.

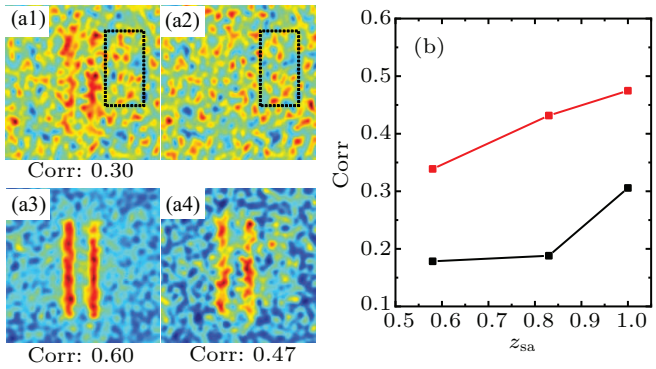


Fig. 2. Experimental results with 3000 measurements when the scattering medium is located at different positions in the test arm. (a1) Ghost image with the disturbance of the scattering medium. (a2) Correlated results between the field after the scattering medium and the reference field. (a3) Ghost image without disturbance. (a4) Recovered image obtained by subtracting (a2) from (a1). (b) The Corr versus z_{sa}, with the red line and black line representing the recovered image and the ghost image, respectively.

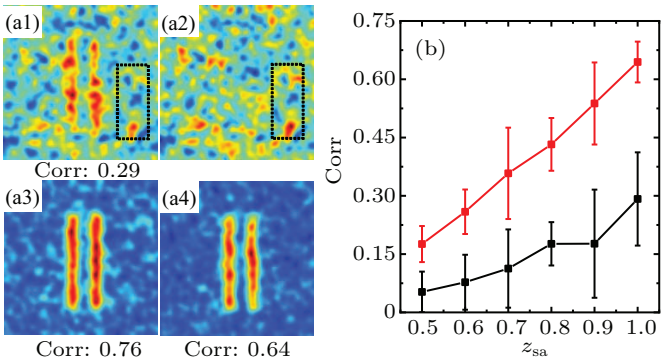


Fig. 3. The numerical results under the scattering medium at different z_{sa}. [(a1), (a2)] The ghost image and the correlated results of the scattering medium, respectively. [(a3), (a4)] The ghost image without disturbance and recovered image, respectively. (b) The Corr versus z_{sa}, with the red line and black line representing the recovered image and the ghost image, respectively.

In addition, the numerical simulations are implemented to further prove the above analysis. Here, $\sigma=1.59$ μm and $s=36$ μm in Eq. (3), and other parameters are consistent with experiments. Figure 3(a1) shows the ghost image. The corresponding correlated results of the scattering medium and recovered images after subtracting operation are presented in Figs. 3(a2) and 3(a4), respectively. Compared with GI without disturbance in Fig. 3(a3), the Corr of result in Fig. 3(a4) can reach 84%. The relationship between Corr of the scheme and the position z_{sa} is shown in Fig. 3(b). In the simulation, each data point is the result of averaging 10 repetitions under the same conditions, and the error bars are displayed at each point. It is shown that the Corr increases when the scattering

medium is closer to the object, which is in good agreement with the experimental results shown in Fig. 2.

Next, we discuss whether the subtraction operation is effective with different scattering concentrations. In our theoretical model, the higher the probability amplitudes (β) of the scattering light is, the higher the concentration of the scattering medium is. Due to the fact that scattering intensity of the scattering medium discussed in Figs. 2 and 3 is $\beta = 0.5$, more β values besides them are considered and other parameters are the same as those in Fig. 2(a). The plot of Corr in the simulation and the experiment for different β is presented in Fig. 4. Here, the red line and black line denote simulation results and experimental results, respectively. Compared the dashed line and the solid line with the same color in Fig. 4. Corr is improved effectively after the subtraction method is used. Moreover, the Corr values of the corresponding recovered images after subtraction operation tend to be stable under different concentrations (see the solid line in Fig. 4), which further proves that the effect of the scattering medium can be eliminated by subtraction operation. Figure 4 also shows that the ghost images from simulations and experiments agree well. After the subtraction operation, the Corr of recovered image from simulations and experiments can reach more than 80% compared with ghost images without disturbance of scattering medium. Nevertheless, it is worth noting that there are discrepancies between the simulation and the experimental results, especially the results of the recovered images and the ghost images without scattering medium disturbance. This is because there are inevitable various noises in the experiment, which are not considered in simulation. The subtraction scheme only aims to eliminate the effects of the scattering medium, other noises still exist, which results in a gap between the black solid line and red solid line in Fig. 4.

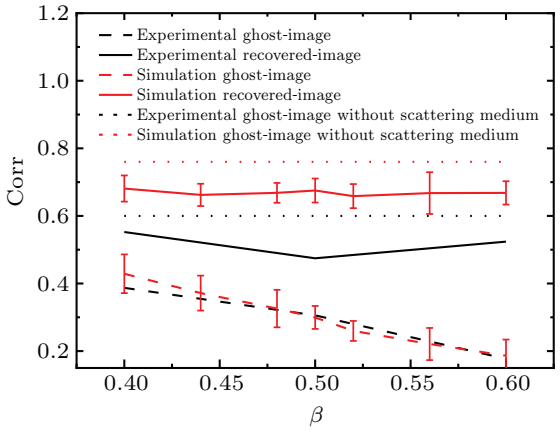


Fig. 4. The Corr of the experimental and simulation results for different β.

Note that DGI[28] can suppress background noise of the ghost image to a certain extend by subtracting the autocorrelation of the reference light field from ghost image. Some researchers may think that the subtraction item is similar to our scheme. Here, the subtraction item in the proposed method is the correlated result between the light field after the scattering medium and the reference light field [see Eq. (4)], which is fundamentally different from that by DGI. To show the superiority of our scheme, we perform imaging processes of DGI and CSGI,[29] which are extensively used, for comparison in Fig. 2(a). Due to the limited number of samplings of CSGI, Fig. 5 shows the reconstructed results from the same array size of 128×160 pixels. One can see that the object information can be retrieved clearly by three methods when the scattering medium is close to the object, while the Corr of our scheme is the highest. When the scattering medium is close to the light source, GI, CSGI, and DGI are less effective (see Figs. 5(a2)–5(c2)), while our scheme can still reconstruct the object image. The results show the superiority of our scheme.

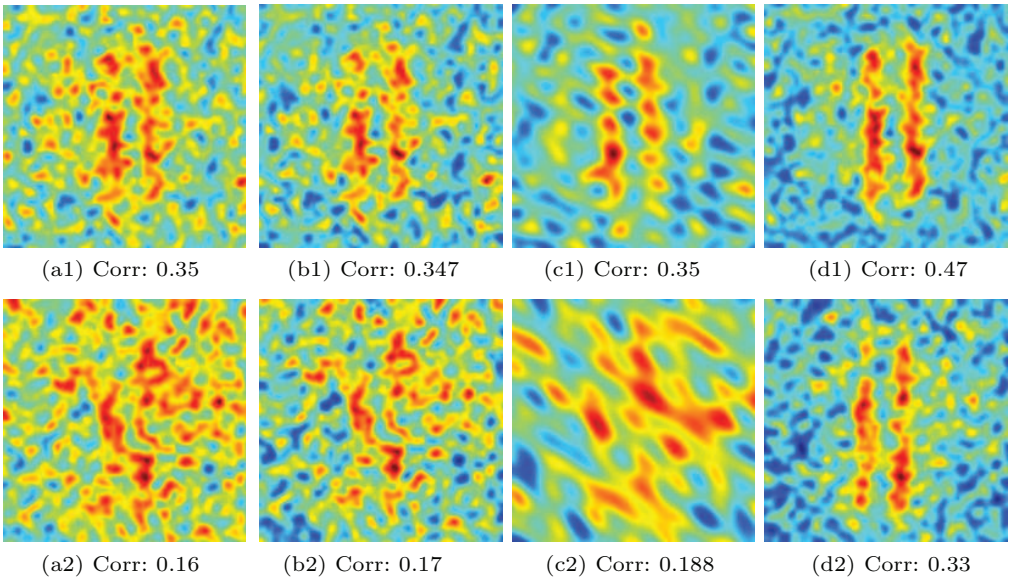


Fig. 5. Experimental results with 3000 measurements by using different methods. The first and second rows correspond to $z_{sa} = 1$ and 0.58, respectively. (a) GI, (b) DGI, (c) CSGI, (d) our scheme.

4. Conclusion

In conclusion, we have theoretically verified that the ghost image with the disturbance of scattering medium can be divided into the image of scattering medium and the image of target object. To prove the conclusion, the disturbance of the scattering medium can be eliminated by subtracting the image of the medium from ghost image. The experimental and simulation results show that the object information can be clearly recovered after the subtraction method. Our scheme avoids the complicated pre-compensation process and it may be applied to the scattering environment, such as medical imaging in biological tissues and endoscopic imaging in multimode fibers.

Acknowledgement

Project supported by the National Natural Science Foundation of China (Grant Nos. 61871431, 61971184, and 62001162).

References

[1] Pittman T B, Shih Y H, Strekalov D V and Sergienko A V 1995 *Phys. Rev. A* **52** R3429
[2] Bennink R S, Bentley S J and Boyd R W 2002 *Phys. Rev. Lett.* **89** 113601
[3] Bai Y F and Han S S 2007 *Phys. Rev. A* **76** 043828
[4] Gong W L 2015 *Photon. Res.* **3** 234
[5] Ferri F, Magatti D, Lugiato L A and Gatti A 2010 *Phys. Rev. Lett.* **104** 253603
[6] Katz O, Bromberg Y and Silberberg Y 2009 *Appl. Phys. Lett.* **95** 131110
[7] Chen W H, An J Y, Li R F, Fu L, Xie G Q, Bhuiyan M Z A and Li K Q 2018 *Future Gener. Comput. Syst.* **89** 78
[8] Wang K, Li K L, Zhou L Q, Hu Y K, Chen Z Y, Liu J and Chen C 2019 *Neurocomputing* **360** 107
[9] Chen J G , Li K L, Bilal K, Zhou X, Li K Q and Yu P S 2019 *IEEE Trans. Parallel Distrib. Syst.* **30** 965
[10] Abdoullahi D and Li Z Y 2019 *Intell Data Anal.* **23** 555
[11] Wang F, Wang H, Wang H C, Li G W and Situ G H 2019 *Opt. Express* **27** 25560
[12] Cheng J 2009 *Opt. Express* **17** 7916
[13] Gong W L and Han S S 2011 *Opt. Lett.* **36** 394
[14] Xu Y K, Liu W T, Zhang E F, Li Q and Yi H 2015 *Opt. Express* **23** 32993
[15] Cizmar T, Mazilu M and Dholakia K 2010 *Nat. Photon.* **4** 388
[16] Lyubov V A and Johannes F D B 2018 *Opt. Lett.* **43** 5427
[17] Lan M Y, Guan D, Gao L, Li J H, Yu S and Wu G H 2019 *Opt. Express* **27** 12957
[18] Shi D F, Fan C Y, Zhang P F, Zhang J H, Shen H, Qiao C H and Wang Y J 2012 *Opt. Express* **20** 27992
[19] Lai P, Wang L, Tay J W and Wang L V 2012 *Nat. Photon.* **9** 126
[20] Conkey D B, Caravaca-Aguirre A M and Piestun R 2012 *Opt. Express* **20** 1733
[21] Martienssen W and Spiller E 1964 *Am. J. Phys.* **32** 919
[22] Chan K W C 2012 *Opt. Lett.* **37** 2739
[23] Jakeman E 1981 *J. Phys. A: Math. Gen.* **15** L55
[24] Hardy N D and Shapiro J H 2011 *Phys. Rev. A* **86** 063824
[25] Gao Y, Bai Y F and Fu X Q 2016 *Opt. Express* **24** 25856
[26] Xu B J, Jiang H Z, Zhao H J, Li X D and Zhu S G 2018 *Opt. Express* **26** 5005
[27] Zeng X, Bai Y F, Shi X H, Gao Y and Fu X Q 2016 *Opt. Commun.* **82** 415
[28] Bina M, Magatti D, Molteni M, Gatti A, Lugiato L A and Ferri F 2013 *Phys. Rev. Lett.* **110** 083901
[29] Durán V, Soldevila F, Irles E, Clemente P, Tajahuerce E, Andrés P and Lancis J 2015 *Opt. Express* **23** 14424